Pinning of magnetic domain walls to structural defects in thin layers within a Heisenberg-type model

Thomas Jourdan, Frédéric Lançon,* and Alain Marty
Département de Recherche Fondamentale sur la Matière Condensée, SP2M, CEA-Grenoble, 38054 Grenoble Cedex 9, France
(Received 15 November 2006; published 22 March 2007)

The interaction between domain walls and structural defects in equiatomic $L1_0$ FePt, antiphase boundaries and microtwins, was investigated by numerical simulations at atomic scale based on a Heisenberg model. It was shown that domain walls are strongly pinned, with depinning fields reaching a few teslas for the thickest microtwins. The potential well of the domain wall pinned in the microtwin is found to be asymmetric as a result of the pinning process. This results in depinning fields depending on the direction of propagation of the wall.

DOI: 10.1103/PhysRevB.75.094422 PACS number(s): 75.70.Ak, 75.40.Mg, 75.60.Ch, 61.72.Nn

I. INTRODUCTION

Recently, some groups proposed innovative ways to use domain-wall motion in magnetologic[1] or data storage[2] devices. The achievement of the targeted functionalities requires both fast and controlled domain motion and reliable wall pinning. Up to now, the largest part of the research effort focused on low anisotropy materials, such as Permalloy. However, materials such as $3d$-$4d$($5d$) equiatomic FePt, FePd, or CoPt, which exhibit large uniaxial magnetocrystalline anisotropy[3] of the order of 10^6 J m^{-3}, may be required at low dimensions to avoid superparamagnetism.

In chemically ordered alloys, structural defects can locally change the environment of the atoms, which leads to different magnetic anisotropies and exchange energies and the pinning of the magnetization. Thus domain-wall motion can be hampered by the presence of structural defects, which gives rise to high magnetic coercivity at the macroscopic scale.

Among these defects, antiphase boundaries (APBs) and microtwins have been shown to prevail in highly ordered FePt(Pd) thin layers.[4] Experimentally, it turns out to be difficult to study the interaction of domains walls with single defects, and up to now only a few results are available.[5] However, numerical simulations give us another insight into the problem by allowing us to isolate a defect and look at the magnetic configuration of a domain wall interacting with it.

Using a Heisenberg-based model, we report in this study a description of microtwins and APBs as pinning sites for domain walls. Configuration of domain walls inside these defects as well as depinning fields are discussed.

II. MODELING

In the Heisenberg model, the exchange energy of a pair of spins i and j, represented by three-dimensional vectors $\boldsymbol{m}_i$ and $\boldsymbol{m}_j$, can be written as

$$E_{ij,e} = -J_{ij}\boldsymbol{m}_i \cdot \boldsymbol{m}_j, \tag{1}$$

where J_{ij} is a coupling constant that can be deduced either from experimental results or from first-principles calculations.

A Zeeman term due to the applied field $\boldsymbol{H}$ is added to this energy. For a spin i, it reads

$$E_{i,Z} = -\boldsymbol{m}_i \cdot \boldsymbol{H}. \tag{2}$$

The magnetic anisotropy energy (MAE) is often taken as a site energy whose analytical expression is given by an expansion in powers of the direction cosines of the magnetization relative to the crystal axes. Using symmetry considerations, it is then possible to carry out some simplifications. However, this model is only suitable for a perfectly ordered material. In order to systematically describe the influence of atomic disorder on the MAE, we have chosen a description proposed by Néel,[6] which stipulates that the MAE of a given atomic site can be written as a sum of contributions of its near neighbors. This model can take into account magnetoelastic effects by letting microscopic parameters depend on the interatomic distances. Since symmetries of the crystal are automatically included via summation, this description is equivalent to the model developed from group theory in the case of a perfect crystal.

The demagnetizing term is computed here as the sum of dipole-dipole interactions. This long-range interaction constitutes the real bottleneck of our atomistic simulations, since computation times are of the order of n^2, where n is the number of spins.

To speed up the computation of the dipolar term, we have implemented one of the fast multipole methods[7] (FMMs). This class of algorithms relies on the efficient grouping of sites via multipole and local expansions, thus reducing the calculation time to the order of n.

The FMM is notably known for its efficient handling of interactions, which can be written by means of the Coulombic kernel,

$$K(\boldsymbol{r}_i,\boldsymbol{r}_j) = \frac{1}{|\boldsymbol{r}_i - \boldsymbol{r}_j|}. \tag{3}$$

To adapt the algorithm to dipolar interactions, we introduce the scalar magnetic potential. For a dipole of magnetic moment $\boldsymbol{m}_i = |\boldsymbol{m}_i|\boldsymbol{u}_i$ located in $\boldsymbol{r}_i$, this potential expressed in $\boldsymbol{r}_j$ has the following form, omitting the prefactor:

$$V(\boldsymbol{r}_j) = \frac{\boldsymbol{m}_i \cdot (\boldsymbol{r}_j - \boldsymbol{r}_i)}{|\boldsymbol{r}_j - \boldsymbol{r}_i|^3} = \boldsymbol{m}_i \cdot \boldsymbol{\nabla}_{\boldsymbol{r}_i}\left(\frac{1}{|\boldsymbol{r}_i - \boldsymbol{r}_j|}\right). \tag{4}$$

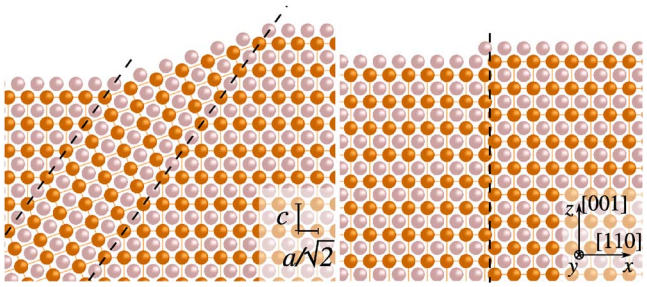

FIG. 1. (Color online) Geometry of a six atomic layer thick microtwin (left) and of an APB (right) at the top of a $L1_0$ FePt thin film.

It is thus possible to use the FMM, as described in Ref. 7 on the condition to replace the Coulombic charges q_i by equivalent charges $|\boldsymbol{m}_i|$ and to consider the kernel

$$K(\boldsymbol{u}_i,\boldsymbol{r}_i,\boldsymbol{r}_j) = \boldsymbol{u}_i \cdot \boldsymbol{\nabla}_{\boldsymbol{r}_i}\left(\frac{1}{|\boldsymbol{r}_i - \boldsymbol{r}_j|}\right), \tag{5}$$

instead of the Coulombic one.

Practically, expressions of multipole expansions of this kernel can be found by taking the gradient of the decomposition of $1/r$ in spherical harmonics. Such an expression has recently also been obtained[8] by gathering the multipole expansions of two opposite charges, whose distance to each other tends to zero while the charge magnitude tends to infinity, thereby creating a dipole.

The total energy of the system, written as the sum of all the previously mentioned contributions, is minimized until the maximum torque on spins is below a given convergence criterion. The energy gradient with respect to one of the spin vectors is the local field applied to this spin. Energy minimizations are performed with conjugate gradient descents with angular coordinates as variables.

III. ATOMIC STRUCTURES

In a $L1_0$ structure, microtwins are formed by the accumulation of stacking faults along the {111} planes of the layer. It corresponds to the propagation of dislocations with a Bürgers vector $\boldsymbol{b}=1/6[a,a,2c]$, where a and c are the lattice parameters of the distorted fcc cell (Fig. 1).

In this study, z is the direction perpendicular to the thin film; x and y are the in-plane directions, corresponding, respectively, to [110] and $[\bar{1}10]$ (Fig. 1). Atomic force microscopy (AFM) observations[4] have shown that microtwins can span over several hundreds of nanometers in the transverse direction y. Therefore, we imposed periodic boundary conditions along y and reduced the number of Fe planes to a minimum of 3 to correctly compute energy terms. The geometry of the domain wall being thus constrained, the validity of this approximation to reproduce three-dimensional (3D) configurations will be discussed in the last part of this study. The system was extended in the x direction by adding an analytical contribution to the dipolar field on each spin coming from two additional semi-infinite layers uniformly magnetized.

Antiphase boundaries were chosen to be in a {110} plane, as shown in Fig. 1. Like the previous system, only three Fe atomic planes were considered in the y direction.

Computations have been carried out for 7.5- and 15-nm-thick layers containing 40 and 80 atomic planes, respectively, along the z direction. The number of atoms in the simulations presented here is around 30 000.

IV. PARAMETERS OF THE MODEL

Both types of defects considered here preserve the close-packed structure. If we neglect elastic relaxation around the microtwin, distances between Fe or Pt atoms are nearly not modified. In the case of an APB, the only defects are antisites. Therefore, magnetoelastic effects do not have to be taken into account, which simplifies the use of Néel's model.

The contribution to the magnetic anisotropy energy from a spin i of a pair (i,j) can be written as an expansion in Legendre polynomials,

$$E_{i,(i,j),a} = \frac{1}{2} l_{i-j}(r_0)(\cos^2 \theta_{i,ij} - 1/3) + \cdots, \tag{6}$$

where r_0 is the distance between i and j and $\theta_{i,ij}$ is the angle between $\boldsymbol{m}_i$ and the vector joining i and j. The expansion is truncated at the second-order term for this study. This is the first nonzero term for a tetragonal unit cell and it permits description of a uniaxial anisotropy as in FePt.

According to *ab initio* calculations,[9,10] Fe atoms induce a small magnetic moment on Pt. Strong spin-orbit coupling of Pt sites is responsible for a high magnetocrystalline anisotropy, which contributes to the anisotropy of Fe sites due to the hybridization between Fe and Pt. It has been shown that suppressing the spin-orbit coupling on Pt sites leads to a considerable decrease in the anisotropy.[10]

Chemical order in FePt thus appears to have a major influence on anisotropy in comparison with the tetragonal distortion ($c/a \approx 0.98$). For a fully ordered material, this distortion does not significantly affect the anisotropy,[9,11] moderately reducing its value.[12,13]

Modeling of anisotropy through the pairs' model has to take into account the major role of Pt sites on the anisotropy. For the sake of simplicity, Pt moments are neglected, which is well justified by first-principles calculations that predict moments of around $3\mu_b$ for Fe and $0.3\mu_b$ for Pt.[10,14] They only act as a source of anisotropy for Fe atoms through the coupling parameter $l_{\text{Fe-Pt}}$. The other parameter $l_{\text{Fe-Fe}}$ is taken as zero.

The summation over the first neighbors of an Fe site in the bulk leads to an anisotropy energy of the form

$$E_{i,a} = K_1 \sin^2 \theta_i, \tag{7}$$

which corresponds to a uniaxial anisotropy, with θ_i the angle between $\boldsymbol{m}_i$ and the normal to the layer and

$$K_1 = -l_{\text{Fe-Pt}} \frac{2(2c^2 - a^2)}{a^2 + c^2}. \tag{8}$$

It can be seen that the tetragonal distortion slightly reduces the value of K_1, in agreement with previous remarks.

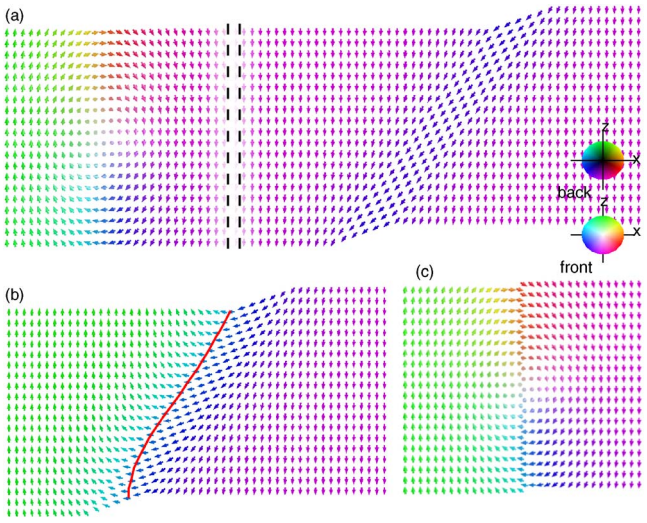

FIG. 2. (Color online) (a) Bloch wall with Néel's caps far from a microtwin. (b) Domain wall pinned in the microtwin (the line indicates the middle of the wall, where the magnetization is along x). (c) Pinned configuration with an antiphase boundary.

Determining exchange coupling constants in FePt for the Heisenberg model is a rather complex task. Several works[14–17] based on *ab initio* calculations have attempted to determine such parameters, but the scattering on the values remains high. A particularly intriguing result is the weak vertical coupling in FePt, which is even found by some calculations to be antiferromagnetic if the material is perfectly ordered.[16,17] The ferromagnetic state is, however, stabilized with the introduction of chemical disorder and the reduction of the tetragonal distortion. Even if the long-range order parameter η is as high as 0.9, for a small lattice tetragonalization ($c/a > 0.97$), the ferromagnetic state is more stable.

In all the simulations presented here, a fully ordered material was kept, the only defects coming from the presence of microtwins or antiphase boundaries. However, all exchange couplings, which were only considered between Fe atoms, were taken as ferromagnetic. Pt atoms poorly contribute to the magnetization and their effect is mainly to mediate interaction between Fe, as pointed out in Ref. 18. This effect was taken into account in effective Fe-Fe coupling constants. We took a small positive vertical coupling constant $J_\perp = J_\parallel/10$ to account for the ferromagnetic coupling that any chemical disorder would experimentally introduce. The constant $J_\parallel$ is the coupling constant with first or second neighbors, both taken equally and strongly ferromagnetic. This in-plane coupling constant was set to 10.8 meV, which is in agreement with first-principles calculations and the experimental value of exchange stiffness constant[19] $A \approx 1 \times 10^{-11}$ J m^{-1}.

V. RESULTS AND DISCUSSION

This set of parameters was used to study the pinning of a domain wall in microtwins and antiphase boundaries. In each case, the initial configuration consists in a Bloch wall on the left of the defect [Fig. 2(a)]. A relaxation leads to the formation of a Bloch core surrounded by the so-called Néel's caps resulting from the dipolar interaction. When a positive field along z is applied, the domain wall propagates and is eventually pinned in the defect, as already pointed out in Refs. 20 and 21 for the microtwin. The geometry of the wall is completely modified in the microtwin, with magnetization lying entirely in the plane of the figure. The domain wall pinned in the APB keeps its structure with only a small contraction of the Bloch core.

A description of the potential-energy wells created by microtwins and antiphase boundaries for a domain wall can be achieved by imposing a constant value of the z component of the magnetization during the minimization process, which sets the position of the domain wall. The difference in energy between the pinned and the free configuration is shown in Fig. 3, where values have been normalized by the energy of the free wall with no dipolar interaction included.

Contrary to the potential well of the antiphase boundary, the potential well of the microtwin is asymmetric. Even if the microtwin has an inversion symmetry, the magnetic configuration breaks this symmetry and depends on the previous direction of propagation of the domain wall. For example, considering a propagation from the left to the right, the configuration on the right of the microtwin rotates smoothly from the easy axis of the defect to the easy axis of the bulk [Fig. 2(b)]. On the left, the rotation is stronger, hence higher exchange and anisotropy energy densities and lower values of depinning field in this direction. This difference in depinning fields can be seen in Fig. 3 since they are proportional to the derivative of the potential well at the inflection points.

The evolution of the depinning field as a function of the thickness of the microtwin (in atomic layers) is shown in Fig. 4. Results of computations without dipolar interaction are also represented and will be discussed later. It can be noticed that strong positive and negative fields are necessary to release the domain wall. After a significant increase of the field for microtwins from one to ten atomic layers, it reaches a limit value. For thick microtwins, indeed, spins inside the defect tend to align along the easy axis and the local environment of the spins remains independent of the number of stacking faults. Remarkably, the absolute value of the depinning field significantly depends on the direction of propagation of the domain wall before the pinning. It can be observed that the depinning field in this direction is up to 25% higher than in the opposite direction.

We now discuss the influence of the vertical exchange coupling $J_\perp$ on depinning field values. For this purpose, we performed computations with a value of $J_\perp$ corresponding to an isotropic exchange stiffness tensor, which is a commonly made hypothesis in micromagnetics. Table I shows depinning fields for an APB and a six atomic layer thick microtwin in a thin film of 80 atomic planes.

It can be seen that a weak coupling is responsible for a sharp increase in the depinning field in comparison with the isotropic case. The magnetic configuration near the depinning threshold, for example, when the domain wall moves to the right of the system, is shown in Fig. 5. The domain wall appears to be released at the bottom of the layer where spins are low coordinated. Given the slanted geometry of the defect, a strong vertical coupling tends to rotate spins at the bottom of the thin film in the direction of the microtwin's

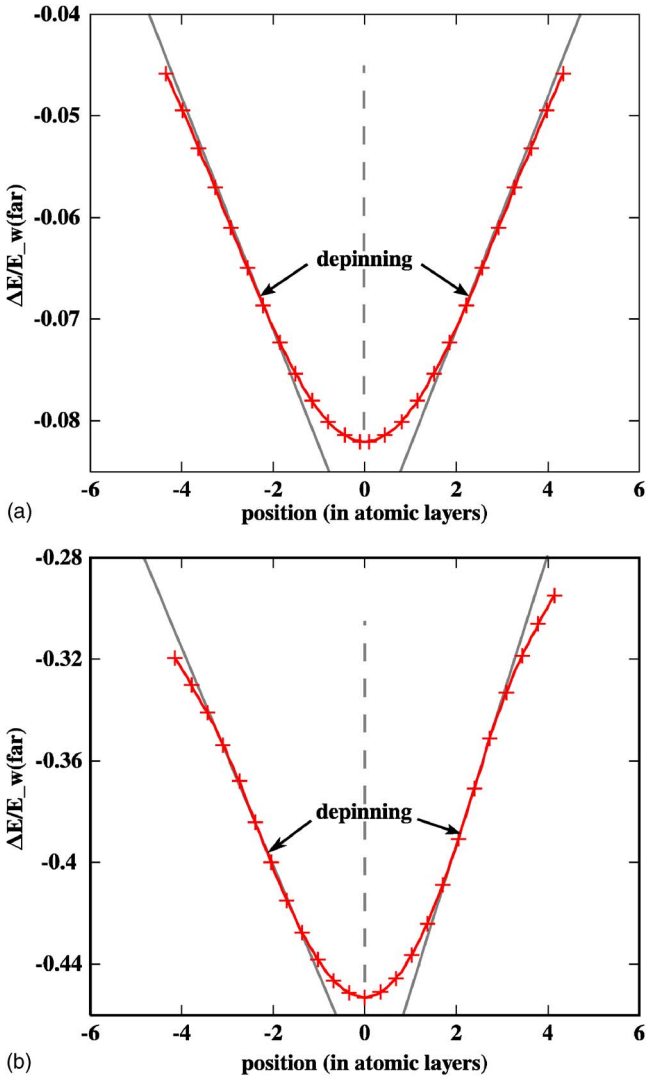

FIG. 3. (Color online) Potential-energy wells for a domain wall pinned in an antiphase boundary (top) or in a six atomic layer thick microtwin (bottom) in the case of a 40 atomic planes thick film. The variation of the energy between the pinned and the free configuration, normalized by the energy of a Bloch wall corresponding to a surface energy density $4\sqrt{AK}$, is plotted as a function of the position of the domain wall, deduced from the z component of magnetization. This position is set to zero when the domain wall is pinned in the defects with no applied field.

TABLE I. Depinning fields on the left (H_l) or on the right (H_r) for a domain wall coming from the left in a six atomic layer thick microtwin and in an APB. Computations are made for strong vertical coupling (isotropic stiffness tensor) and weak coupling ($J_\perp = J_\parallel/10$). The layers contain 80 atomic planes.

	Microtwin		APB	
	H_l (T)	H_r (T)	H_l (T)	H_r (T)
Weak coupling	−2.00	2.50	−0.60	0.60
Isotropic coupling	−1.15	1.90	−0.55	0.55

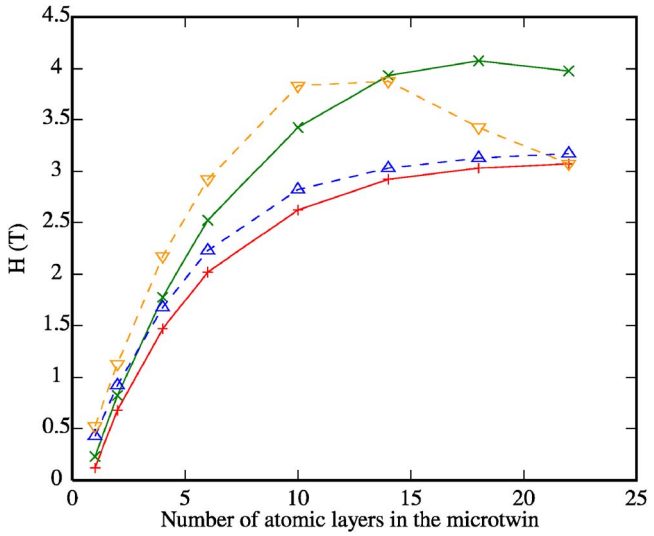

FIG. 4. (Color online) Variation of the absolute value of the depinning field as a function of the microtwin's thickness (in atomic layers), with the hypothesis that the domain wall comes from the left of the system. Results are shown for dipolar term omitted (depinning on the left: △ and on the right: ▽) and included (depinning on the left: + and on the right: ×). The layers contain 80 atomic planes.

spins. This rotation facilitates the depinning by an applied field.

The value of the vertical coupling also affects the depinning field for an APB but to a lesser extent. A weak coupling results in a vertical contraction of the Bloch core and more spins align in the plane perpendicular to the domain wall and the surface, which is found to be a locally easy plane for the anisotropy. The energy of the wall is then reduced, which leads to higher depinning fields.

When the dipolar interaction is not taken into account, the decrease of the depinning field for microtwins of more than 15 atomic layers (Fig. 4) is due to a different depinning process. In this case, a tilted domain wall is created into the defect at the bottom of the layer. The depinning occurs when the wall propagates upwards under positive magnetic field. For the microtwins considered here, when the dipolar term is included, the creation of such a domain wall where the mag-

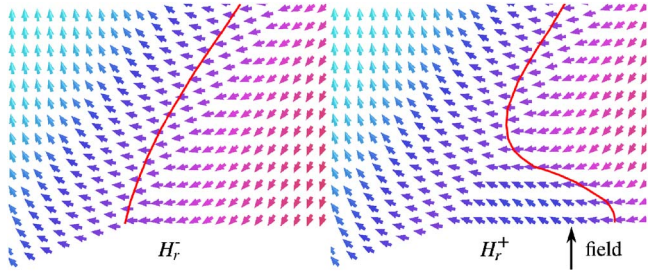

FIG. 5. (Color online) Magnetic configuration for low vertical coupling, just below the depinning field (left, H_r^-) and at the beginning of the depinning (right, H_r^+). It can be noticed that the magnetization is entirely in the plane of the figure (the color is a guide to the eye and the lines are the location where the magnetization is perpendicular to the field).

netization rotates in the plane is not observed, for it would involve the presence of volumic magnetic charges.

The vertical exchange length, beyond which dipolar interactions prevail, is only 0.8 nm. Therefore, an effect of the dipolar term on the depinning field can be expected even for the thinnest layers considered here. For a microtwin containing six atomic layers, switching off the dipolar term yields to an increase of nearly 12% and 20% in the depinning field for 7.5- and 15-nm-thick layers, respectively. Without including dipolar interactions, the depinning field is independent of the thickness of the system, thus it can be concluded that the long-ranged dipolar term cannot be neglected in these simulations, especially for films significantly thicker than the exchange length.

The geometry used in this study constrains the depinning to occur as a whole, parallel to the y direction, whereas it may start by a local deformation of the domain wall through thermal activation.[5] However, in case the width of the system does not exceed a few tens of nanometers, the computations presented here are expected to correctly reproduce three-dimensional simulations at 0 K. A simple argument for this assumption consists in considering a domain wall held by a pinning site on the border of a system invariant along z. This domain wall can be regarded as a surface of energy density $\gamma=4\sqrt{AK}$. By analogy with hydrostatics, the surface energy corresponds to a tension which gives the ability to resist the "magnetic pressure" $2MH$, where H is the applied field. Minimizing the energy leads to a domain wall of radius $R=\gamma/(2MH)$. This radius is found to be a little more than 10 nm for $H=1$ T due to the strong values of anisotropy and exchange. This supports the hypothesis of a parallel depinning for sufficiently small systems, as in nanowires.

VI. CONCLUSIONS

Using a Heisenberg-based atomic model, numerical computations have been carried out on model systems containing extended defects, microtwins and antiphase boundaries, in highly ordered FePt. Simulations have shown a strong pinning of domain walls by these defects. This result underlines the crucial role played by structural defects in materials with a high magnetocrystalline anisotropy. For any application requiring a tight distribution of propagation fields, a well controlled microstructure is then a prerequisite.

We described original effects such as an asymmetric potential well seen by a domain wall pinned in a microtwin, which results in depinning fields depending on the direction of depinning. The originality of this phenomenon, which is ascribed to the tilted anisotropy axis, is due to the dependence of the shape of the potential-energy well on the direction of propagation of the wall before the pinning.

ACKNOWLEDGMENT

The authors would like to acknowledge Yves Samson for useful suggestions about the manuscript.

*Corresponding author. Electronic address: frederic.lancon@cea.fr

[1] D. A. Allwood, G. Xiong, M. D. Cooke, C. C. Faulkner, D. Atkinson, N. Vernier, and R. P. Cowburn, Science **296**, 2003 (2002).
[2] S. Parkin, U.S. Patent No. 7,031,178 (18 April 2006).
[3] H. Kanazawa, G. Lauhoff, and T. Suzuki, J. Appl. Phys. **87**, 6143 (2000).
[4] D. Halley, Y. Samson, A. Marty, P. Bayle-Guillemaud, C. Beigné, B. Gilles, and J. E. Mazille, Phys. Rev. B **65**, 205408 (2002).
[5] J. P. Attané, D. Ravelosona, A. Marty, Y. Samson, and C. Chappert, Phys. Rev. Lett. **96**, 147204 (2006).
[6] L. Néel, J. Phys. Radium **15**, 225 (1954).
[7] H. Cheng, L. Greengard, and V. Rokhlin, J. Comput. Phys. **155**, 468 (1999).
[8] N. L. Gorn and D. V. Berkov, J. Magn. Magn. Mater. **272–276**, 698 (2004).
[9] P. Ravindran, A. Kjekshus, H. Fjellvaag, P. James, L. Nordström, B. Johansson, and O. Eriksson, Phys. Rev. B **63**, 144409 (2001).
[10] T. Burkert, O. Eriksson, S. I. Simak, A. V. Ruban, B. Sanyal, L. Nordström, and J. M. Wills, Phys. Rev. B **71**, 134411 (2005).
[11] S. Ostanin, S. S. A. Razee, J. B. Staunton, B. Ginatempo, and E. Bruno, J. Appl. Phys. **93**, 453 (2003).
[12] J. B. Staunton, S. Ostanin, S. S. A. Razee, B. Gyorffy, L. Szunyogh, B. Ginatempo, and E. Bruno, J. Phys.: Condens. Matter **16**, 5623 (2004).
[13] J. Lyubina, I. Opahle, K.-H. Müller, O. Gutfleisch, M. Richter, M. Wolf, and L. Schultz, J. Phys.: Condens. Matter **17**, 4157 (2005).
[14] A. Kashyap, R. Skomski, A. K. Solanki, Y. F. Xu, and D. J. Sellmyer, J. Appl. Phys. **95**, 7480 (2004).
[15] H. Zeng, R. Sabirianov, O. Mryasov, M. L. Yan, K. Cho, and D. J. Sellmyer, Phys. Rev. B **66**, 184425 (2002).
[16] G. Brown, B. Kraczek, A. Janotti, T. C. Schulthess, G. M. Stocks, and D. D. Johnson, Phys. Rev. B **68**, 052405 (2003).
[17] O. N. Mryasov, J. Magn. Magn. Mater. **272–276**, 800 (2004).
[18] O. N. Mryasov, U. Nowak, K. Y. Guslienko, and R. W. Chantrell, Europhys. Lett. **69**, 805 (2005).
[19] S. Okamoto, N. Kikuchi, O. Kitakami, T. Miyazaki, Y. Shimada, and K. Fukamichi, Phys. Rev. B **66**, 024413 (2002).
[20] J. P. Attané, Y. Samson, A. Marty, D. Halley, and C. Beigné, Appl. Phys. Lett. **79**, 794 (2001).
[21] J. P. Attané, Y. Samson, A. Marty, J. C. Toussaint, G. Dubois, A. Mougin, and J. P. Jamet, Phys. Rev. Lett. **93**, 257203 (2004).